Optics Communications 356 (2015) 373–377

Contents lists available at ScienceDirect

Optics Communications

journal homepage: www.elsevier.com/locate/optcom

Sensing characteristics based on Fano resonance in rectangular ring waveguide

Zhiquan Chen [a,b], Hongjian Li [a,*], Shiping Zhan [a], Zhihui He [a], Boxun Li [a], Hui Xu [a]

[a] College of Physics and Electronic, Central South University, Changsha 410083, China
[b] College of Communication and Electronic Engineering, Hunan City University, Yiyang 413000, China

ARTICLE INFO

Article history:
Received 30 June 2015
Received in revised form
3 August 2015
Accepted 10 August 2015

Keywords:
Surface Plasmon Polaritons
Fano resonance
Sensor
Sensitivity
Figure of merit

ABSTRACT

Sensing characteristics based on Fano resonance in a rectangular ring resonator with a stub are investigated numerically. Simulation results show that a sharp and asymmetric Fano-line shape emerges in the proposed structure. Through tuning the width and length of the stub, it is found that the width and length play an important role in optimizing the sensing characteristic. Using the sharp and asymmetric Fano-line shape a highly sensitive plasmonic nanosensor with the sensitivity of 1000 nm/RIU and a tunable figure of merit (FOM) can be attained. The maximum FOM can reach up to 992,800 when the stub length $d=120$ nm, width $l=130$ nm and the refractive index difference $\Delta n=0.05$, which is larger than that in previous reports. In addition, the results show that a larger FOM can be obtained by tuning the stub width than tuning its length. The proposed model and results provide guidance for fundamental research of the plasmonic nanosensor applications and designs.

1. Introduction

Surface Plasmon Polaritons (SPPs), known as controlling light at the nanoscale due to their capability to overcome the diffraction limit [1], has attracted enormous researches, such as the biomedicine [2], optical filter [3], solar cell [4], and so on. A metal–dielectric–metal (MDM) waveguide, which supports the propagation of SPPs in the metal–dielectric interface and manipulates light on a subwavelength scale can be regarded as an ideal integrated photonic device [5–6]. Applications based on MDM waveguide have been widely reported, such as plasmon induced transparency (PIT) [7–10], optical switch [11], slow light devices [12–15], plasmonic waveguide filters [16–20], and plasmonic sensors [21–24].

Recently, Fano resonances have been also observed in MDM waveguides, which are known as a fundamental resonant effect, discovered by Ugo Fano [25], originate from the interference of the discrete state and continuum state [26], and possess a distinctly sharp and asymmetric line profile. The specific feature of the Fano resonance has shown great sensitivity and larger figure of merit (FOM) and has promising applications in sensors. Lu et al. reported an MDM waveguide side-coupled with a pair of nanoresonators with a sensitivity of about 900 nm/RIU and a FOM of about 500 [22]. Chen et al. showed a rectangular ring metal–insulator–metal waveguide with a baffle and achieved a FOM of about 6838 [24]. Nevertheless, these researches mainly focused on the sensing property of specific structure parameters; the sensing optimization based on tuning the structure parameters is seldom discussed.

In this paper, a rectangular ring resonator loaded with a stub is proposed and the optical transmission properties of the structure are investigated numerically by the Finite Difference Time Domain (FDTD). Simulation results show that a sharp and asymmetric Fano resonance line-shape can be obtained. Through tuning the length (d) and width (l) of the stub and the refractive index (n) of the dielectric, FOM is investigated in the proposed MDM waveguide structure in detail. The results show that FOM changes with d, l and Δn. The structure can work as an excellent plasmonic sensor with a sensitivity of about 1000 nm/RIU and a FOM of about 992,800 when $d=120$ nm, $l=130$ nm, and $\Delta n=0.05$ at $\lambda=1088$ nm, which is larger than that in previous reports [22,24]. The results show that a larger FOM can be obtained by tuning the stub width than by tuning its length.

2. Structure and simulations

The proposed MDM waveguide structure, which consists of a rectangular ring resonator coupled with a bus waveguide, is schematically shown in Fig. 1(a). A stub is loaded in the middle of the horizontal branch of the rectangular ring resonator. Fig. 1 (b) shows the 2-dimensional schematic structure of Fig. 1(a), where the turquoise and white areas represent Au and air, respectively. The width of the bus waveguide and the rectangular

* Corresponding author.
E-mail address: lihj398@126.com (H. Li).

http://dx.doi.org/10.1016/j.optcom.2015.08.020
0030-4018/

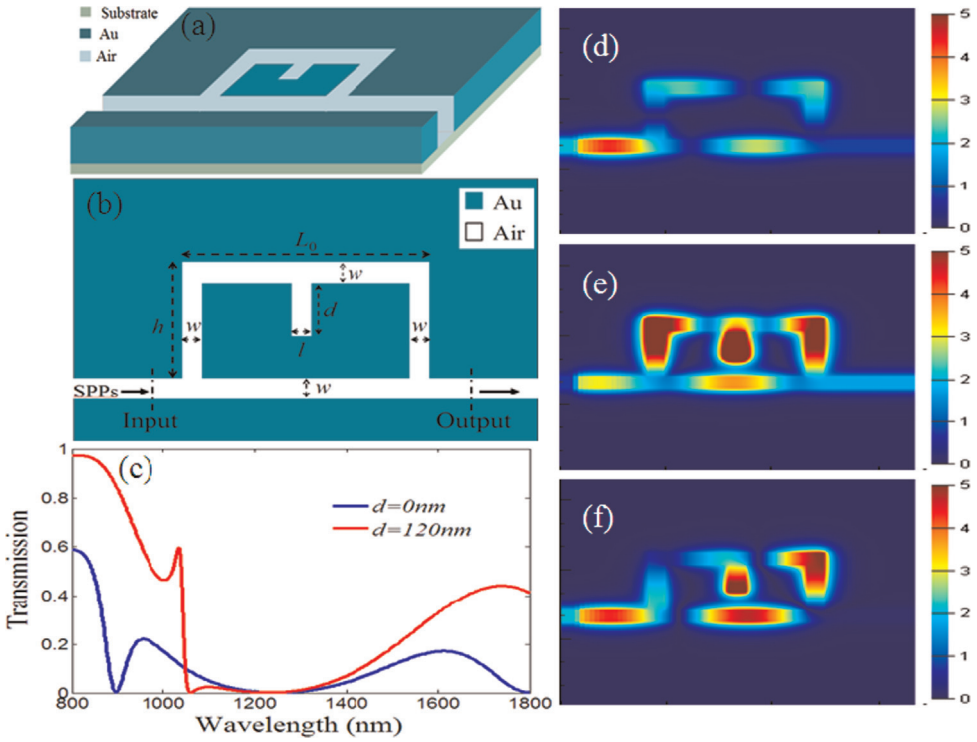

Fig. 1. Schematic of the rectangular ring resonator with a stub: (a) 3-dimensional. (b) 2-dimensional. (c) Transmission spectra of rectangular ring resonator without a stub (blue curve) and with a stub with width $l=50$ nm, length $d=120$ nm (red curve). (d) Magnetic field distribution of structures without stub at $\lambda=1033$ nm. Magnetic field distribution of structures with stub: (e) $\lambda=1033$ nm. (f) $\lambda=1061$ nm. (For interpretation of the references to color in this figure legend, the reader is referred to the web version of this article.)

ring resonator is w, and the length and height of the rectangular ring are L_0 and h, respectively. l and d represent the width and length of the stub, respectively.

The properties of Fig. 1(b) are numerically investigated using the two-dimensional FDTD method. When an incident pulse is input, the propagating SPP wave, which is confined in the metal–dielectric interface, may be coupled into the rectangular ring resonator and the stub. In the simulation, the permittivity ε_m of Au can be approximately defined by the Drude model: $\varepsilon_m(\omega)=\varepsilon_\infty-\omega_p/(\omega^2+i\omega\gamma_p)$, where ω stands for the angle frequency of the incident wave, $\varepsilon_\infty=3.7$, $\omega_p=1.37\times10^{16}$ rad/s is the bulk plasmon frequency, and $\gamma_p=4.08\times10^{13}$ rad/s stands for the damping rate, which characterizes the absorption loss. These values are obtained by fitting the experimental results [27]; the parts colored in white are chosen to be air with permittivity $\varepsilon_0=1$ for simplicity. Optical transmission properties of the proposed structure are investigated in time domain when fix $w=50$ nm, $L_0=500$ nm, and $h=250$ nm. Transmission spectra of the plasmonic waveguide are tuned by adjusting the width and length of the stub. Transmittance is calculated by $T=P_{out}/P_{in}$, where P_{in} and P_{out} stand for the input and output power, respectively.

The transmission spectra of the structure without and with a stub are shown by the blue and red curves in Fig. 1(c), respectively. It is clear that the transmission spectrum (blue curve) becomes sharp and asymmetric (red curve) when the structure is loaded by a stub ($l=50$ nm, $d=120$ nm). For the asymmetric spectra, the transmittance of the SPPs varies sharply from the peak to valley with a small wavelength shift. The field distributions of the peak ($\lambda=1033$ nm) and the valley ($\lambda=1061$ nm) are displayed in Fig. 1 (e) and (f), respectively. The field distribution of the structure without stub at $\lambda=1033$ nm is displayed in Fig. 1(d). At $\lambda=1033$ nm, when without the stub, most of the power is reflected back to the input, and almost no power transports to the output. On the contrary, when loaded with a stub, strong field distributions are obviously observed in the rectangular ring resonator and the stub, a part of power transports to the output. The resonant mode of the rectangular ring is changed by the stub. At $\lambda=1061$ nm, there are also no power transports to the output, most of which is trapped in the rectangular ring resonator and the stub; the others are reflected back to the input.

3. Transmission characteristics and analysis

As shown in Fig. 1(d)–(f), the incident light waves can be reflected back and forth in the proposed structure, the rectangular ring resonator, with the stub just like an FP resonator, which results in a sharp and asymmetric Fano resonance [26]. The accumulated phase delay per round trip in this FP resonator is $\Delta\varphi=k(\omega)\cdot2(L+d)+\theta$, where $k(\omega)=2\pi\cdot n_{eff}/\lambda$ is the angular wave number at frequency ω, L is the effective length of rectangular ring, θ is the phase shift brought by the reflection in the resonator and n_{eff} is the effective refractive index of the SPP mode in the resonator. When $\Delta\varphi=m\cdot2\pi$ (m is an integer), the resonance wavelengths λ_m can be expressed as

$$l_m = 2n_{eff}\times(L+d)/(m-q/2p) \quad (1)$$

It is worth noting that n_{eff} and L are related to the resonance wavelength λ_m and play an important role in controlling resonance wavelength and transmission in this structure.

The evolution of transmission characters is depicted in Fig. 2. Fig. 2(a) shows the Fano resonance wavelength has a red-shift with the increment of the stub length from 110 nm to 140 nm when the width is fixed at $l=50$ nm. This phenomenon can be explained by Eq. (1); with the increase of stub length d, the effective length of the resonator increased, which means λ_m became larger. Fig. 2(b) shows the resonance wavelength has a blue-shift

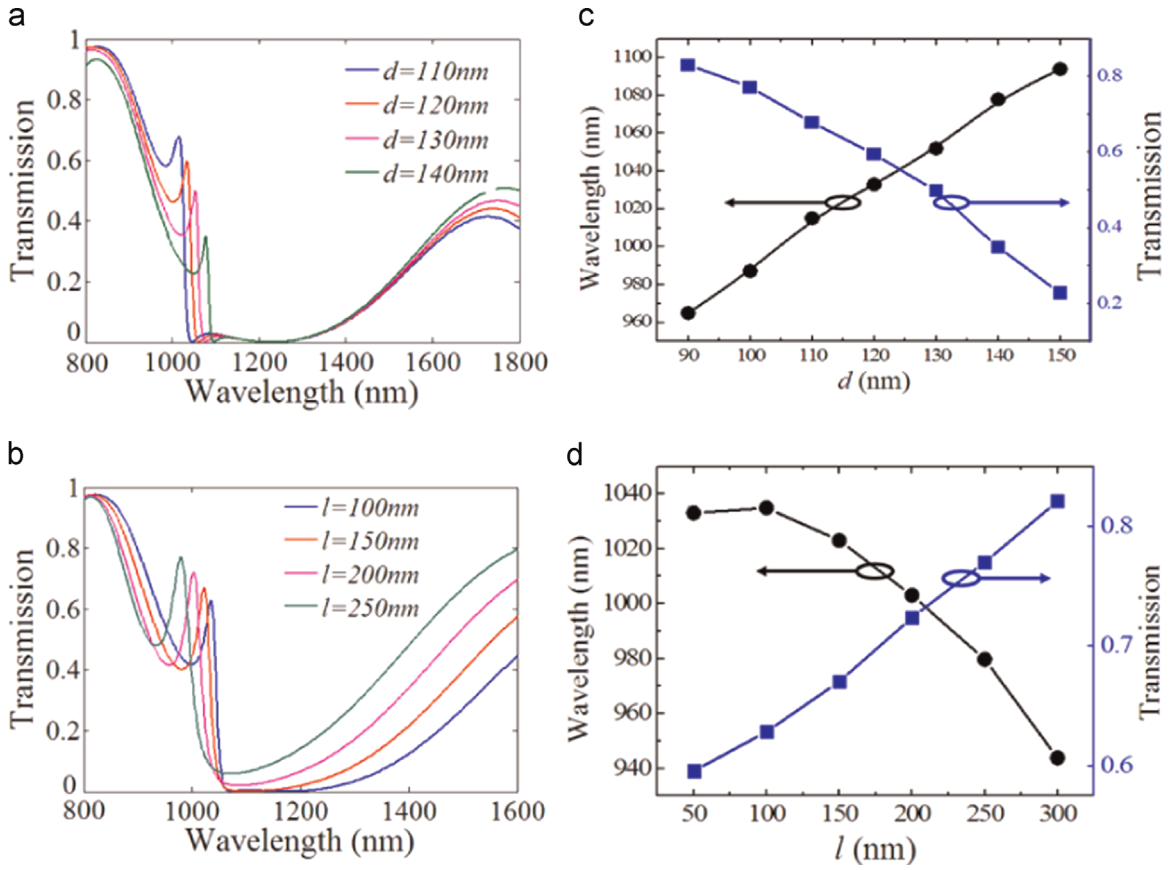

Fig. 2. Transmission characteristics of rectangular ring waveguide with loaded stub: (a) $l=50$ nm, $d=110$–140 nm. (b) $d=120$ nm, $l=100$–250 nm. Numerical of the peak wavelength and transmission: (c) $l=50$ nm, $d=90$–150 nm. (d) $d=120$ nm, $l=50$–300 nm.

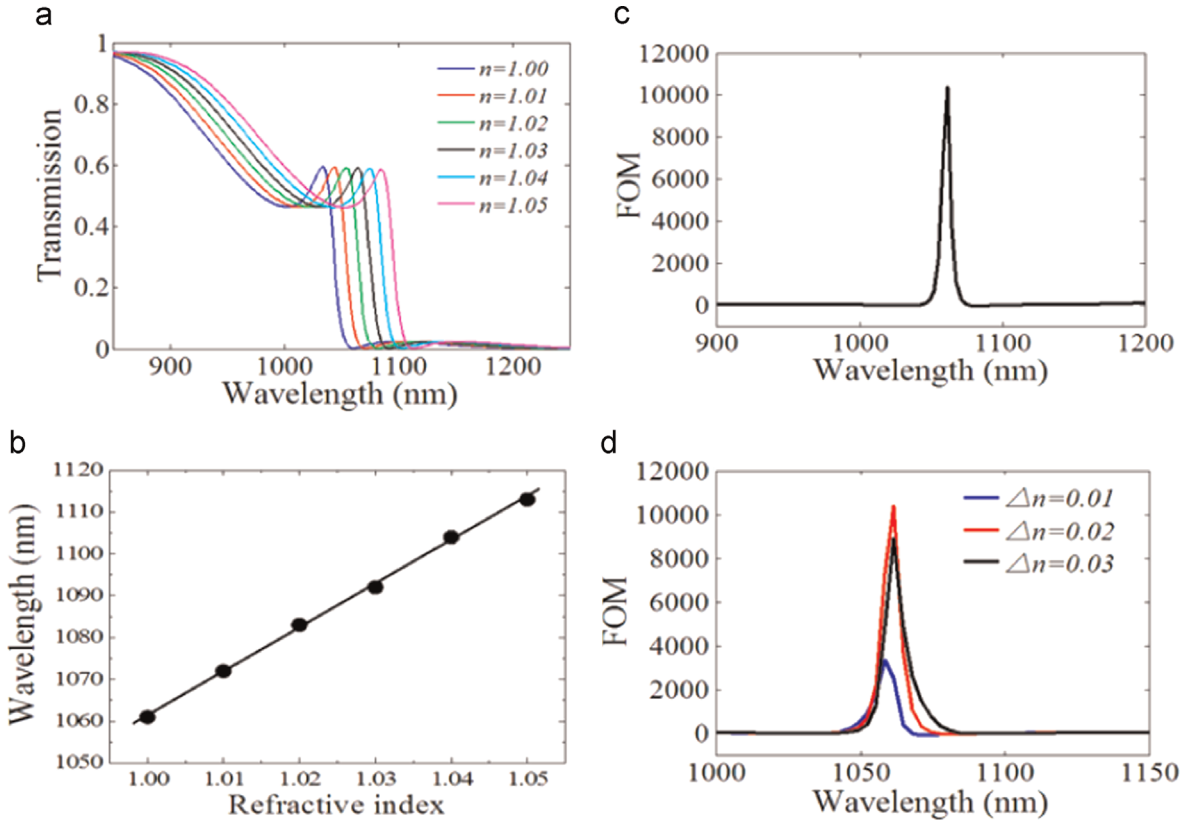

Fig. 3. (a) Transmission spectra with different refractive index when $l=50$ nm, $d=120$ nm. (b) Resonance wavelength as a function of refractive index. FOM as a function of wavelength: (c) $\Delta n=0.02$. (d) $\Delta n=0.01$–0.03.

with the increment of the stub width from 100 nm to 250 nm when the length is fixed as $d=120$ nm, which can be attributed to the decrease of n_{eff}· when the width of the resonator is increased [28]. Fig. 2(c) and (d) is the numerical representation of the peak wavelength and transmission of Fig. 2(a) and (b), respectively. Additional simulations results indicate that a Fano-line shape can be obtained when the length of the stub $d=80$–160 nm, and the width $l=20$–250 nm with the dimension of the rectangular ring unchanged.

4. Sensing characteristics based on Fano resonance

The resonance wavelength has a red-shift when there is an increase in the refractive index of the dielectric which fills the resonance cavities [29–30]. Because of the sharp peak with narrow line width, Fano resonance is considered to be very sensitive to the surrounding environment variation [22]. Fig. 3(a) shows the transmission spectra of the structure for different refractive indices from 1 to 1.06 with a step of 0.01; the width and length of the loaded stub are 50 nm and 120 nm, respectively. As the refractive index increases, the transmission spectrum exhibits a sensitive shift; this feature provides potential applications in nanoscale sensing [31]. The sharp asymmetric Fano line shape enhances the sensitivity of the sensor. The sensitivity is the shift in the wavelength of the Fano resonance dip per unit change of refractive index (RIU) [32], which can expressed as RIU$=\Delta\lambda/\Delta n$ (nm/RIU). Fig. 3(b) shows that the wavelength of the Fano resonance responds linearly to the refractive index. The resonance wavelength shifts from 1061 nm to 1113 nm with the refractive index increasing from 1.00 to 1.05; the calculated sensitivity is about 1000 nm/RIU, which is larger than that reported for plasmonic sensors [22,31–32]. For better quantification, the plasmonic sensor detects the relative intensity change $\Delta I/I$ at a fixed wavelength λ_0 induced by a small index change Δn. The figure of merit (FOM), which is another key factor of Fano resonance, is defined as FOM$=\max[\Delta I/(I\cdot\Delta n)]$ [33], where I represents the output transmission intensity. Fig. 3(c) depicts the calculated FOM at different wavelengths when the refractive index changed from 1.00 to 1.02. It can be found that the max FOM is about 10,380 at $\lambda=1062$ nm. Fig. 3(d) shows the FOM at different wavelengths when $\Delta n=0.01$, 0.02, and 0.03, respectively. The FOM of the structure increases from 3341 to 10,380 and then decreases to 8902 at $\lambda=1062$ nm, the change of FOM can be attributed to the increments of ΔI and Δn not being unified – ΔI first increases and then decreases with the increasing of Δn.

To further investigate the tuning of FOM in the proposed structure, the effects of different parameters for FOM are investigated in detail. Fig. 4(a) and (b) shows FOM as a function of Δn. When the width of the stub is fixed at $l=50$ nm, FOM for the stub length $d=80$, 100, 110, 120 nm is shown in Fig. 4(a). With increase of Δn, FOM first increases and then decreases in the case of $d=80$, 100, 110, and 120 nm; the Δn, which corresponds to the maximum FOM, decreases with the increase of d. In addition, when $d=110$ nm, the maximum FOM of the structure approximates to 11,500. Fig. 4(b) shows FOM for the stub width $l=80$, 90, 100, and 110 nm and the length fixed at $d=120$ nm. The evolution of FOM has the same trend as Fig. 4(a) as the increases of Δn. Nevertheless, the Δn corresponding to the maximum FOM shows an increasing trend as l increases. For a given width of $l=110$ nm, the maximum FOM of the structure reaches 85,820. Fig. 4(c) and (d) shows FOM as a function of the length d and width l of the

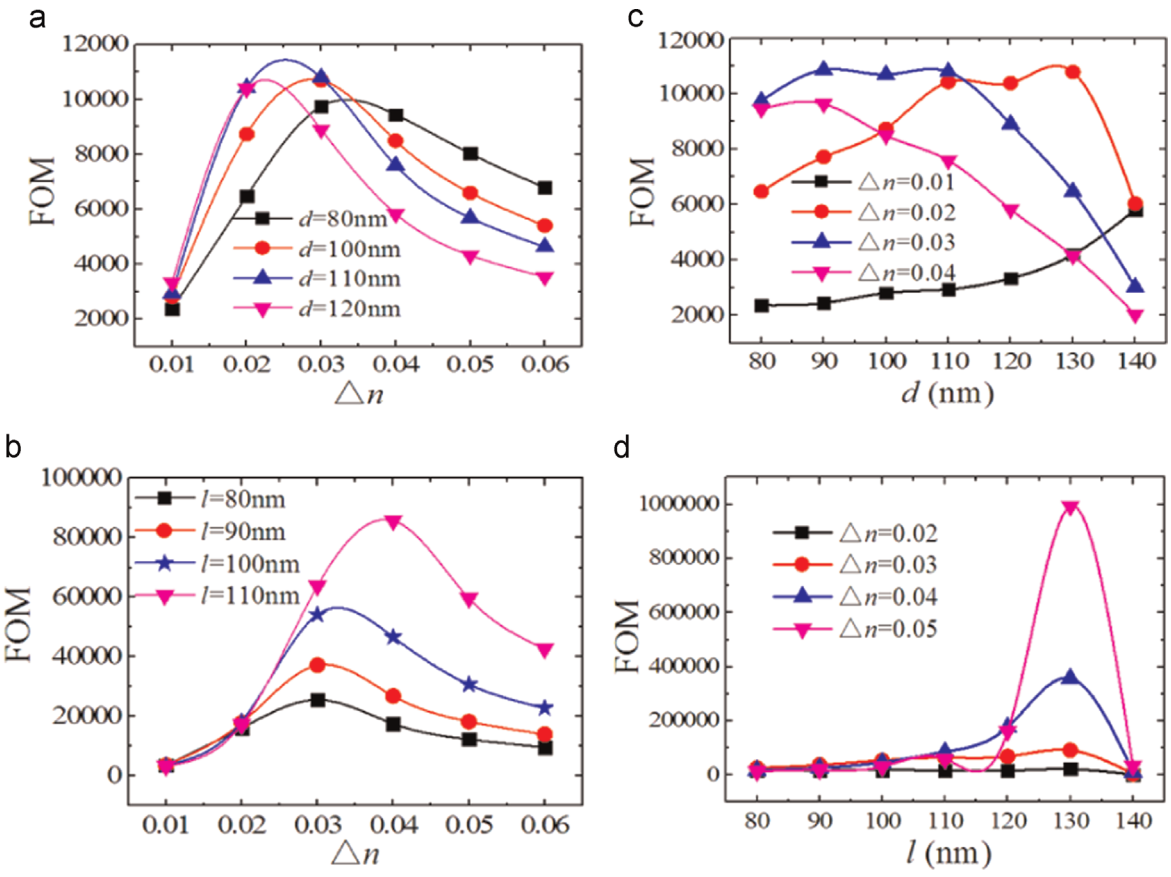

Fig. 4. FOM as a function of Δn: (a) $l=50$ nm, $d=80$–120 nm. (b) $d=120$ nm, $l=80$–110 nm. (c) FOM as a function of d when $l=50$ nm. (d) FOM as a function of l when $d=120$ nm.

stub, respectively. Fig. 4(c) show FOM reaches 10,000 at the ranges of d from 80 nm to 110 nm and 110 nm to 130 nm when $\Delta n=0.03$ and $\Delta n=0.02$, respectively. Fig. 4(d) shows that the FOM obviously changes in the range of l from 120 nm to 140 nm. It also depicts that FOM enlarges with the increase of Δn, for the case of $l=130$ nm, $\Delta n=0.05$, the FOM of this structure can reach to 992,800, which is larger than that mentioned in previous reports [22,24]. As mentioned above, we can also conclude that tuning the width can obtain a larger FOM than tuning the length of the stub, which can provide some references for the design of a sensitive sensor.

5. Conclusion

In summary, a rectangular ring resonator with a stub is proposed and investigated by FDTD. Simulation results show that a sharp and asymmetric Fano line-shape emerges in the proposed structure. The transmission spectrum is manipulated by tuning the width and length of the stub; results show that the transmission spectrum has a red-shift with the increase of d when fixed at $l=50$ nm and a blue-shift with the increases of l when fixed $d=120$ nm. Finally, by adjusting the parameters Δn, l, d, a highly sensitive plasmonic nanosensor with the sensitivity of 1000 nm/RIU and a tunable FOM can be obtained. The maximum FOM reaches 992,800 when $d=120$ nm, $l=130$ nm, and $\Delta n=0.05$, which is larger than in previous reports. It was also found that tuning the stub width can get a higher FOM than tuning its length. This work may provide some references in the designing of a plasmonic nanosensor.

Acknowledgments

This work was funded by the Fundamental Research Funds for the Central Universities of Central South University (Grant no. 72150050429), and the National Natural Science Foundation of China (Grant no. 61275174).

References

[1] D.K. Gramotnev, S.I. Bozhevolnyi, Nat. Photonics 4 (2010) 83.
[2] J. Yang, J. Lee, J.Y. Kang, S.J. Oh, H.J. Ko, J.H. Son, K. Lee, J.S. Suh, Y.M. Huh, S. Haam, Adv. Mater. 21 (2009) 4339.
[3] I. Zand, M.S. Abrishamian, T. Pakizeh, IEEE J. Sel. Top. Quantum Electron. 19 (2013) 4600505.
[4] H.A. Atwater, A. Polman, Nat. Mater. 9 (2010) 205.
[5] C.J. Min, G. Veronis, Opt. Express 17 (2009) 10757.
[6] Y. Huang, C.J. Min, G. Veronis, Opt. Express 20 (2012) 22233.
[7] S.P. Zhan, D.M. Kong, G.T. Cao, Z.H. He, Y. Wang, G.J. Xu, H.J. Li, Solid State Commun. 174 (2013) 50.
[8] Z.H. He, H.J. Li, S.P. Zhan, G.T. Cao, B.X. Li, Opt. Lett. 39 (2014) 5543.
[9] G.T. Cao, H.J. Li, Y. Deng, S.P. Zhan, Z.H. He, B.X. Li, Opt. Express 22 (2014) 25215.
[10] S.P. Zhan, H.J. Li, G.T. Cao, Z.H. He, B.X. Li, H. Xu, Plasmonics 9 (2014) 1431.
[11] Z.J. Zhong, Y. Xu, S. Lan, Q.F. Dai, L.J. Wu, Opt. Express 18 (2010) 79.
[12] G.T. Cao, H.J. Li, S.P. Zhan, H.Q. Xu, Z.M. Liu, Z.H. He, Y. Wang, Opt. Express 21 (2013) 9198.
[13] Y. Huang, C.J. Min, G. Veronis, Appl. Phys. Lett. 99 (2011) 143117.
[14] H. Lu, X.M. Liu, G.X. Wang, D. Mao, Nanotechnology 23 (2012) 444003.
[15] S.P. Zhan, H.J. Li, G.T. Cao, Z.H. He, B.X. Li, H. Yang, J. Phys. D: Appl. Phys. 47 (2014) 205101.
[16] I. Zand, A. Mahigir, T. Pakizeh, M.S. Abrishamian, Opt. Express 20 (2012) 7516.
[17] X. Zhai, L. Wang, L.L. Wang, X.F. Li, W.Q. Huang, S.C. Wen, D.Y. Fan, J. Opt. 15 (2013) 055008.
[18] G.X. Wang, H. Lu, X.M. Liu, D. Mao, L.N. Duan, Opt. Express 19 (2011) 3513.
[19] G.T. Cao, H.J. Li, Y. Deng, S.P. Zhan, Z.H. He, B.X. Li, Plasmonics 9 (2014) 1163.
[20] S.P. Zhan, H.J. Li, G.T. Cao, Z.H. He, B.X. Li, H. Xu, J. Opt. Soc. Am. 31 (2014) 2263.
[21] S. Roh, T. Chung, B. Lee, Sensors 11 (2011) 1565.
[22] H. Lu, X.M. Liu, D. Mao, G.X. Wang, Opt. Lett. 37 (2012) 3780.
[23] J.J. Chen, Z. Li, Y.J. Zou, Z.L. Deng, J.H. Xiao, Q.H. Gong, Plasmonics 8 (2013) 1627.
[24] Z. Chen, L.N. Cui, X.K. Song, L. Yu, J.H. Xiao, Opt. Commun. 340 (2015) 1.
[25] U. Fano, Phys. Rev. 124 (1961) 1866.
[26] A.E. Miroshnichenko, S. Flach, Y.S. Kivshar, Rev. Mod. Phys. 82 (2010) 2257.
[27] E.D. Palik, Handbook of Optical Constants of Solids, Academic Press, Boston, 1985.
[28] J. Park, H. Kim, B. Lee, Opt. Express 16 (2008) 413.
[29] H. Lu, X.M. Liu, D. Mao, Y.K. Gong, G.X. Wang, Opt. Lett. 36 (2011) 3233.
[30] H. Lu, X.M. Liu, D. Mao, L.R. Wang, Y.K. Gong, Opt. Express 18 (2010) 17922.
[31] N. Liu, T. Weiss, M. Mesch, L. Langguth, U. Eigenthaler, M. Hirscher, C. Sönnichsen, H. Giessen, Nano Lett. 10 (2010) 1103.
[32] N. Liu, M. Mesch, T. Weiss, M. Hentschel, H. Giessen, Nano Lett. 10 (2010) 2342.
[33] J. Becker, A. Trügler, A. Jakab, U. Hohenester, C. Sönnichsen, Plasmonics 5 (2010) 161.